(9) Starkweather, H. W. J. Appl. Polym. Sci. 1980, 25, 139.
(10) This program is available from the Quantum Chemistry Program Exchange, Department of Chemistry, Indiana University, Bloomington, IN. Refer to: QCPE 1975, 7, 318.
(11) Wertz, D. H.; Allinger, N. L. Tetrahedron 1974, 30, 1579.
(12) Allinger, N. L.; Tribble, M. T.; Miller, M. A.; Wertz, D. H. J. Am. Chem. Soc. 1971, 93, 1637.
(13) Flory, P. J. "Statistical Mechanics of Chain Molecules"; Interscience: New York, 1969; pp 136-140.
(14) Zerbi, G.; Gussoni, M.; Ciampelli, F. Spectrochim. Acta, Part A 1967, 23A, 301.
(15) Setterquist, R. A. U.S. Patents 3 932 307 and 3 950 269.
(16) Fukui, K.; Hirai, I. British Patent 1 568 659.
(17) Willbourn, A. H. Trans. Faraday Soc. 1958, 54, 717.

Simultaneous Static and Dynamic Light Scattering

Siegfried Bantle, Manfred Schmidt, and Walther Burchard*

Institut für Makromolekulare Chemie der Universität Freiburg, D-7800 Freiburg, West Germany. *Received March 2, 1982*

ABSTRACT: A modified photon correlation spectrometer that allows the simultaneous recording of dynamic and static light scattering is described. Details for a precise alignment are given. The utility of the equipment is demonstrated with four well-characterized polystyrene samples and two polystyrene latices. Excellent agreement with literature values is obtained for the linear, monodisperse polystyrene samples. The apparent diffusion coefficient, D_{app}, of the large latex particle (481 nm) exhibits no angular dependence up to an angle of 120°. At larger angles a drastic drop of D_{app} is observed, which is shown to be caused by 2% reflection of the primary beam at the solution–glass boundary and at the refractive index matching bath–air boundary. For the smaller latex (91 nm) the back-scattering has a somewhat different influence on D_{app}, which is almost negligible.

Introduction

Quasi-elastic or dynamic light scattering (QLS) has become in recent years a powerful technique for the characterization of polymers.[1] It favorably supplements the now long and well established static or frequency-integrated light scattering (ILS). Measurements of the weight-average molecular weight M_w, the mean square radius of gyration $\langle S^2\rangle_z$, the second virial coefficient A_2, the diffusion coefficient D_z or the corresponding hydrodynamic radius $\langle R_h^{-1}\rangle_z$, and the coefficient k_d of the concentration dependence of the diffusion coefficient have become routine, and in some cases where the molecules have dimensions on the order of the wavelength of the light, information on the shape and architecture of the molecules can be gathered from the angular distribution of the particle scattering factor $P_z(q)$ and the reduced first cumulant Γ/q^2 of the scattering intensity correlation function ($q = (4\pi/\lambda)\sin(\theta/2)$). Recently, it has been shown that a combination of data from both light scattering techniques produces two parameters of particular value.[2] These are the ratio

$$\rho = \langle S^2\rangle_z^{1/2}\langle R_h^{-1}\rangle_z \quad (1)$$

and the coefficient C in the general relationship

$$\Gamma/q^2 = D_z(1 + C\langle S^2\rangle_z q^2 - \ldots) \quad (2)$$

Both quantities are significant parameters for the extent of branching, chain rigidity, the existence of loops, and the molecular polydispersity. A third quantity, k_{fo}, is obtained by combination of several parameters in the following equations:[3-6]

$$k_f + k_d = 2A_2M_w + \bar{\nu}_2 \quad (3)$$

$$k_f = k_{fo}(N_A V_h/M_w^3) \quad (4)$$

$$V_h = (4\pi/3)R_h^3 \quad (5)$$

In these equations k_f is the coefficient of the concentration dependence of the frictional coefficient f, given by

$$f = f_0(1 + k_f c + \ldots) \quad (6)$$

The amplitude factor k_{fo} depends on the extent of coil interpenetration. In the theory of Pyun and Fixman,[4] $k_{fo} = 7.16$ for hard spheres and 2.23 for fully interpenetrating coils, i.e., the Θ state.

To date, the parameters from static and dynamic light scattering have been determined separately using different instruments, and in order to evaluate the quantity ρ, one had to use measurements from different laboratories. The combination of such data for $\langle S^2\rangle_z$ and $\langle R_h^{-1}\rangle_z$ for PMMA[7] and polystyrene (PS)[8] in Θ solvents led to ρ ratios that were 16–23% lower than predicted theoretically,[3] and similar deviations have been found for both polymers in a good solvent.[7,9] These deviations raise the question to what extent they may be caused by systematic errors introduced by different instruments and different authors. The relative errors in both techniques are fairly low (8% for $\langle S^2\rangle_z$ and 3% for D_z or $\langle R_h^{-1}\rangle_z$), and ρ should be measurable to an accuracy of ±5% or better, provided the systematic errors could be avoided. In principle, this should be possible since with most autocorrelators the ILS intensity is also recorded.

In general, the rule holds true that a real optimization can only be achieved with one instrument and for only one quantity of measurement. The two light scattering techniques are no exception to this. For instance, in QLS the choice of a rather small scattering volume (not larger than 0.2^3 mm^3) is imperative for a good signal-to-noise ratio,[10] whereas ILS can be more easily carried out with precision if the scattering volume is large. Nevertheless, we have adapted our photon correlation spectrometer to ILS, which has involved us in a series of painfully precise adjustments of our spectrometer. We are now able to perform combined static and dynamic light scattering measurements to a high precision with the same instrument at the same time, and this has promoted us into a position where we can measure the properties of slowly changeable systems, e.g., the coagulation of micelles or a change of properties with temperature.

Meanwhile the combined static and dynamic light scattering has become routine in our laboratory and a number of different systems have been studied, including

0024-9297/82/2215-1604$01.25/0

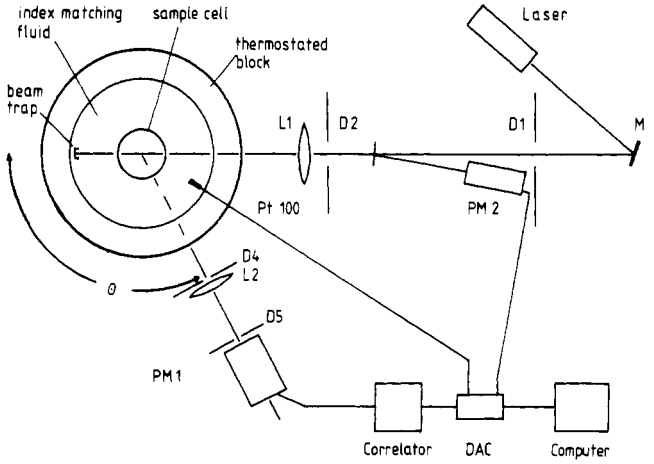

Figure 1. Schematic diagram of the light scattering spectrometer. Explanations are given in the text.

the solution properties of linear and branched polymers in solution,[11] the structure of κ-casein micelles,[12] and thermally reversible associating or gelling systems.[13] The details of the spectrometer modifications are described herein, and the quality of the instrument is demonstrated with some specially selected examples.

Experimental Section

Light Scattering Apparatus. A schematic diagram of the light scattering apparatus is shown in Figure 1. A laser beam (either a krypton ion laser, Spectra Physics, Model 165, or a He–Ne laser, Spectra Physics, Model 124) is adjusted by the mirror M to pass through two pinholes D1 and D2. This guarantees that the laser beam is aligned parallel to the optical table. The lens L1 (focal length 200 mm) focuses the beam to the center of the goniometer, where the beam waist is calculated to be 0.2 mm. The sample cell in the center of the goniometer is surrounded by an index-matching and temperature-controlled bath, consisting of a special glass cylinder filled with pure toluene. The features of the glass cylinder, manufactured by Hellma, Müllheim, West Germany, are a high-quality optical glass and plane-parallel optical windows for the primary beam in order to avoid lens effects. The index-matching bath is placed in a copper block, which is thermostated by a circulating fluid. In addition, an electric heater is connected to the sample holding block.

The photomultiplier PM1 records the scattering intensity and is placed on the goniometer arm, where it can be aligned in all three directions of space. The goniometer has been improved to a centricity of 0.01 mm over the experimentally accessible angular range of 10–150°.

A small fraction of the primary beam is reflected onto a light conductor line by a thin optical-quality glass plate. It then passes through a monochromator (which eliminates extraneous light from the room) and is recorded by the photomultiplier PM2. Finally, the signal is transferred by an interface to an on-line computer (see Data Transfer).

Optical Alignment. ILS measurements require a most accurate placement of the scattering volume in the center of the goniometer. This means that the focused primary beam and the optical axis of the photomultiplier PM1 have to be adjusted precisely. This is achieved by a specially designed cell,[14] consisting of a thin metal wire (copper or steel, diameter 0.2 mm) exactly centered in a glass cell containing toluene. The laser beam is adjusted to pass through the middle of this cell, so that the diffraction pattern of the wire appears symmetrical. For the adjustment of the photomultiplier PM1 we use a well-centered needle that just touches the beam. The tip of the needle is smaller than the beam waist, and its diffraction pattern, which can be observed on the pinhole D5 by a special eyepiece, should not change on variation of the scattering angle. A slight correction in height is necessary after this adjustment since the needle only touches the primary beam and cannot be placed as a point scatterer in the center of the beam (as is required in principle). The accuracy of the final adjustment is checked by the angular

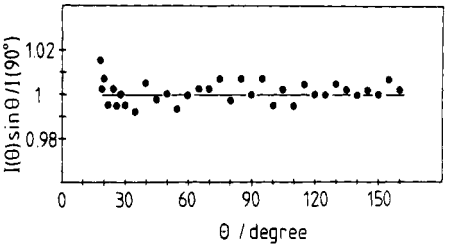

Figure 2. Scattering intensity I_θ/I_{ref} for toluene as a function of the scattering angle θ. Scattering volume 0.008 mm^3.

independence of the Rayleigh ratio of a well-clarified toluene solution. The image of the correlation volume on the photodiode is achieved by a pinhole–lens–pinhole system. The first pinhole D4 (diameter 0.2 mm) controls the size of the scattering volume, while the lens L2 (focal length 100 nm) together with pinhole D5 (diameter 0.2 mm) determines the angular aperture, which in our case was smaller than 0.05°.

Data Transfer. The commerically available Data Aquisition interface[15] controls the start–stop–reset functions of a 96-channel Malvern K7023 correlator and transfers the correlation data to a Hewlett-Packard 9825 on-line computer. The interface also transfers the temperature of the refractive index matching bath, determined ty a PT100 thermoresistive element, and the counts of the reference photomultiplier PM2 to the correlator. At present, two other feasibilities, i.e., recording and transfer of the solution pH and an analog signal, are not used.

Sample Preparation. Three commercial polystyrenes (Toyo Soda samples F80, F126, and F288) and one prepared by Huber[16] (M_w = 99 500, M_w/M_n = 1.07) were dissolved in toluene that had been distilled and dried over sodium. All samples were clarified with a Beckman ultracentrifuge Model L5 and a swinging-bucket rotor, applying a special floating technique[17] where aqueous cesium chloride was used as a density agent. The solutions were centrifuged for 1–3 h at 5000–15 000 rpm, depending on the molecular weight of the samples.

Two polystyrene latex products from Dow Chemical Co. (diameters 481 and 91 nm, respectively) were used for a further check of the instrument. The latex suspensions were diluted with water and then filtered through Milipore filters of 800- and 120-nm, pore size, respectively. The concentrations of the latices ranged from approximately 10^{-4} to 10^{-2}% solid latex. The exact concentrations were not determined since our results exhibited no concentration dependence.

Light Scattering Experiments. Before the start of each experiment the optical alignment is checked by measuring the angular dependence of the scattering intensity of a highly purified and clarified toluene solution. When in the autocorrelation mode, the channel 00 of the Malvern correlator collects the total counts arriving at PM1, and this is compared to the total counts arriving at the reference PM2 in the same time interval. After the usual sine correction of the scattering volume, an angular-independent ratio of the two count rates is obtained for toluene with a well-adjusted instrument (see Figure 2). The Rayleigh ratios of the samples are calculated as follows:

$$R_\theta = (I_\theta/I_{ref})_{sample}/(I_\theta/I_{ref})_{tol}(U_v)_{tol} \quad (7)$$

where $(I_\theta/I_{ref})_{sample}$ and $(I_\theta/I_{ref})_{tol}$ are the ratios of counts of the scattered and the primary intensities for the sample and for toluene, respectively. $U_v = 1.2 \times 10^{-5}$ cm^2 is the Rayleigh ratio of toluene at λ_0 = 647 nm for vertically polarized light.[18] A value of the refractive index increment dn/dc = 0.106 was used for polystyrene in toluene at λ_0 = 647.1 nm wavelength.[19]

Results

In order to prove the applicability and the advantage of our instrument, we chose only well-characterized samples. Four polystyrene samples of different molecular weights were studied in toluene at 20 °C by simultaneous ILS and QLS. The well-adjusted spectrometer allowed measurement of $\langle S^2\rangle_z^{1/2}$ down to 10 nm.[16] A typical example of a Berry plot[20] for the ILS (where the root of Kc/R_θ is plotted) and the corresponding Zimm plot of the

Table I

sample	$10^{-6}M_w$	10^7D_z, cm²/s	10^4A_2, (cm³ mol)/g²	k_d, cm³/g	$\langle S^2\rangle_z^{1/2}$, nm	$\langle 1/R_h\rangle_z^{-1}$, nm	ρ^a
Huber[16]	0.099	4.45	6.8	19	12	8.2	1.46
F80	0.783	1.34	2.8	113	38.6	27.0	1.43
F126	1.28	1.01	2.7	173	52.0	36.2	1.44
F288	2.89	0.53	2.35	432	84.4	68.6	1.23

[a] $\rho = \langle S^2\rangle_z^{1/2}\langle 1/R_h\rangle_z$.

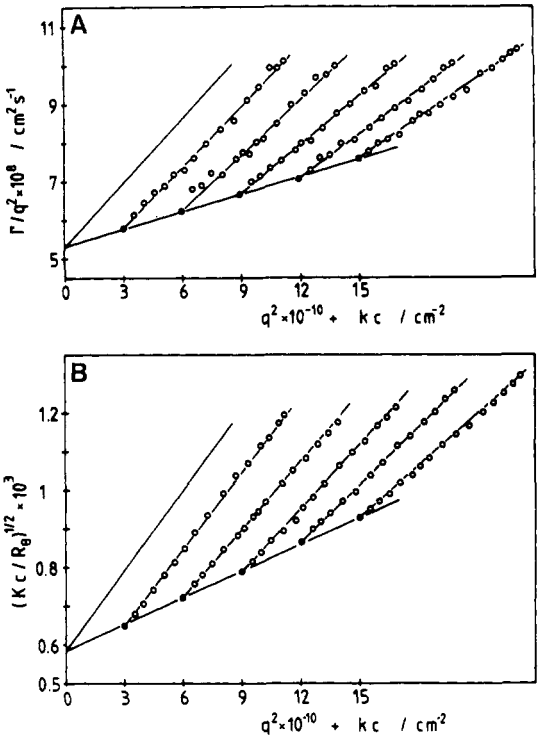

Figure 3. Simultaneously measured QLS and ILS data for the polystyrene sample F288 at five concentrations ranging from 0.2 × 10^{-3} to 1.0 × 10^{-3} g/cm³. (A) Zimm plot of the reduced first cumulant, which exhibits a slope C for zero concentration and a slope D_zk_d for zero-angle extrapolation. (B) Berry plot of the static light scattering data.

reduced first cumulant Γ/q^2 are shown in Figure 3 for the F288 sample. The results for all four samples are listed in Table I. The diffusion coefficients, the radii of gyration, and the second virial coefficients agree well with values that can be read off from the relationships given by Raczek and Meyerhoff,[21] with the exception of the diffusion coefficient of the F288 sample, which was significantly too small, whereas M_w and $\langle S^2\rangle_z$ were found as expected. At present, we have no explanation for this behavior.

For a further check of our instrument two latex samples with particle diameters of 481 and 91 nm were examined in water at 20 °C. Theory predicts no angular dependence of the reduced first cumulant for monodisperse hard spheres,[22] and the time correlation function should be a single exponential. The particle scattering factor of the static light scattering, however, can show a very pronounced angular distribution, depending on the size of the spheres.[23,24] Such behavior was indeed observed for the 481-nm latex over a wide angular region, yielding a zero-angle extrapolated diffusion coefficient D_z = 8.1 × 10^{-9} cm² s^{-1} and a hydrodynamic radius $\langle 1/R_h\rangle_z^{-1}$ = 266 nm. However, as seen in Figure 4, a sudden decrease of the reduced first cumulant was observed at angles larger than 120°. This effect was accompanied by an increasing deviation of the time correlation function from a single exponential, as indicated by an increase of the second cumulant (see Table II). In addition, at those high angles

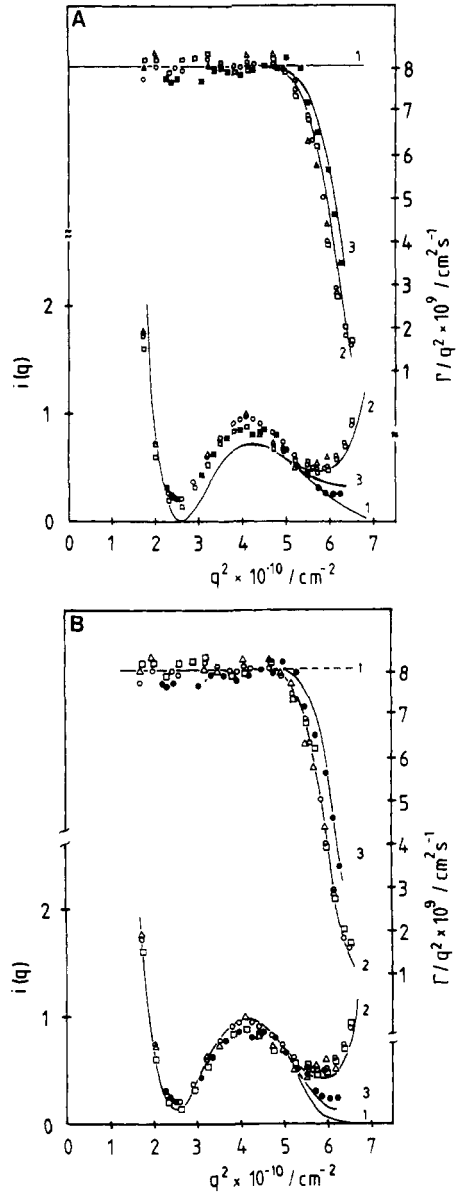

Figure 4. (A) Simultaneously measured QLS and ILS data for the 481-nm Dow latex at four concentrations: (△) $c_1 \cong 10^{-4}$% solid latex; (×) $c_2 \cong 2c_1$; (□) $c_3 \cong 10c_1$; (○) $c_4 \cong 20c_1$. c_1, c_3, and c_4 were measured without a special light trap, and c_2 was measured with a beam trap. The solid curves were calculated with the Rayleigh–Gans approximation for the scattering intensities and assuming a latex radius of 280 nm and no back-reflection (1), 1.5% back-reflection (2), and 0.4% back-reflection (3). (B) The meaning of the symbols is as in part A. The solid lines were calculated taking account for Mie scattering and assuming a latex radius of 265 nm and no back-reflection (1), 2% back-reflection (2), and 0.25% back-reflection (3).

the simultaneous recorded static scattering intensity was significantly higher than that calculated from the particle scattering factor using the Rayleigh[23]–Gans[24] approximation or using the scattering intensities given by Pangonis and Heller,[25] thus taking proper account for possibly oc-

Table II
Values of the Normalized Second Cumulant for Different Scattering Angles[a]

angle, deg	μ_2 [b]	angle, deg	μ_2 [b]
60	0.03-0.05	110	0.01-0.03
65	0.01-0.04	115	0.04-0.08
70	0.02-0.04	120	0.12-0.19
75	0.01-0.02	125	0.18-0.22
80	0.02-0.04	130	0.28-0.39
85	0.04-0.06	135	0.60-0.72
90	0.02-0.03	140	0.55-0.90
95	0.02-0.05	145	1.65-1.75
100	0.02-0.03	150	1.61-1.80
105	0.05-0.06		

[a] The range quoted for the second cumulant at one angle holds for all three latex concentrations measured without a beam trap. [b] $\mu_2 = 2\Gamma_2/\Gamma^2$.

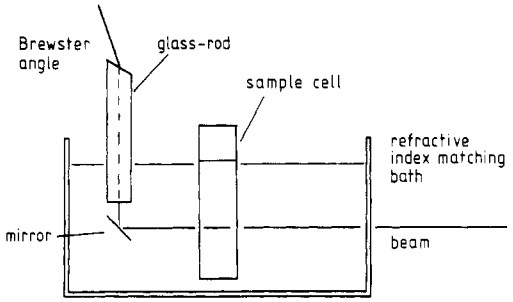

Figure 5. Schematic diagram on a beam trap. Mirror M placed in the index-matching fluid reflects the primary beam into a glass rod with the same refractive index as the fluid. Brewster's angle avoids beam reflection at the glass rod–air boundary.

curring Mie scattering. Similar behavior is commonly observed when back-scattering occurs due to reflection of the primary beam at the solution–glass boundary and at the glass–air boundary of the refractive index matching bath.

Model calculations reveal that the first maximum and the second minimum of the static scattering intensity are strongly dependent on the fraction of the reflected primary beam, while the first minimum is essentially unaffected by back-scattering and depends only on the particle size. In the Rayleigh–Gans approximation the best fit to our ILS data was obtained for a latex radius of 280 nm (which is slightly greater than R_h) and a fraction of 1.5% reflection of the primary beam reentering the correlation volume (see Figure 4A, lower curve 2). However, a qualitatively better fit was obtained by accounting for Mie scattering (see Figure 4B, lower curve 2), yielding a latex radius of 265 nm (which now matches exactly R_h) and 2% of the primary beam reflection being in back-scattering.

In order to minimize the back-scattering we constructed a special beam trap, which avoids reflection of the primary beam at the glass–air boundary of the refractive index matching bath without heating up the index-matching fluid at high primary beam intensities. The beam trap is schematically shown and explained in Figure 5. When the measurements for the 481-nm latex were repeated at one concentration, the ILS data indicated a reduction of the reflected light down to 0.4% using the Rayleigh–Gans approximation (Figure 4A, lower curve 3) and down to 0.25% accounting for Mie scattering (Figure 4B, lower curve 3). Apparently, this 0.25% reflection originates from the solution–glass boundary of the sample cell and can hardly be avoided.

Back-scattering also influences the dynamic scattering, and the magnitude of this effect can be calculated as

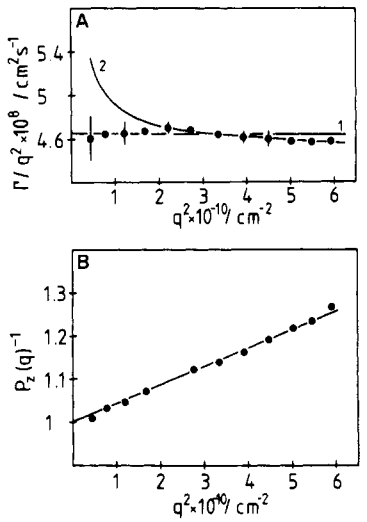

Figure 6. (A) Reduced first cumulant for the 91-nm Dow latex. The solid line 1 is expected without back-scattering and the solid line 2 with 1.5% back-scattering. (B) The inverse particle scattering factor is plotted against q^2, yielding a mean square radius of gyration $\langle S^2 \rangle_z^{1/2} = 35.7$ nm.

follows. The correlation function of monodisperse, hard spheres, including the effect of back-scattering, may be written as (see Appendix)

$$g_1(t) = B_1 \exp(-q^2Dt) + B_2 \exp(-(q^{*2}/q^2)q^2Dt) \quad (8)$$

From this relationship the reduced and normalized first cumulant is obtained as

$$\Gamma/(q^2D_z) = D_{app}/D_z = [P(q) + P(q^*)]^{-1}[P(q) + P(q^*)(I_r/I_p)(q^{*2}/q^2)] \quad (9)$$

where $P(q)$ is the particle scattering factor, q and q^* are the scattering vectors at angles θ and $180° - \theta$, respectively, and I_r/I_p is the ratio of the reflected to the primary intensity. Evidently, the measured decrease of D_{app} at large angles is caused by the second exponential, which decays much more slowly, depending on q^{*2}/q^2. Assuming again 1.5% and 2% reflection of the primary beam, the upper curves 2 in Figure 4A,B are obtained for the scattering intensities due to Rayleigh–Gans and due to Mie, respectively. The corresponding measurement with the installed beam trap is well described by the upper curves 3 in Figure 4A,B, for which again 0.4% and 0.25%, respectively, primary beam reflection was assumed. Accounting for Mie scattering yielded again a slightly better fit to the data.

The measured latex diameters of 530 (ILS) and 532 (QLS) nm do not coincide with the value of 481 nm given by Dow Chemical Co. Similar deviations have been reported by other groups for this particular sample,[26] and we cannot offer an explanation so far.

The result for the 91-nm latex is shown in Figure 6 and yields a hydrodynamic radius of $\langle 1/R_h \rangle_z^{-1} = 46.1$ nm (Dow 45.5 nm) and a radius of gyration of $\langle S^2 \rangle_z^{1/2} = 35.7$ nm, leading to a ratio $\rho = 0.774$, which agrees well with the theoretical value of 0.775 for a hard sphere. When eq 8 is applied to the smaller latex particle, we find a different behavior. At large angles the effect of back-scattering is predicted to be not larger than the experimental error. This occurs because the particle scattering factor for the 91-nm latex decreases by only 25% within the q range of our measurement. At small angles, however, the second exponential in eq 8 decays very rapidly (by a factor q^{*2}/q^2 faster than the first exponential), and this should cause the reduced first cumulant to increase as q decreases.

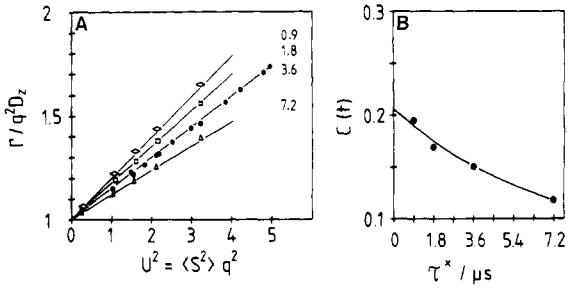

Figure 7. (A) Normalized reduced first cumulant as a function of $u^2 = \langle S^2 \rangle_z q^2$. The various slopes $C(t)$ originate from different sampling time, $\tau^* = \tau \sin^2(\theta/2)$, in units of μs as shown on the curves. $\tau^* = 3.6$ μs represents the optimal sampling time suggested by Jakeman et al.[10] (B) The slopes $C(t)$ in part A are plotted against the sampling time τ^*, yielding a zero-time extrapolated slope $C = 0.2$.

Figure 6A shows good agreement with theory for all angles larger than 70°. As the scattering angle becomes less than 70°, a decrease of D_{app} is found instead of the expected increase (solid line 2 in Figure 6A), although the difference is hardly greater than the experimental error. This behavior is a consequence of the large value of q^{*2}/q^2 at small angles, such that the second exponential has decayed almost to zero at a time when the first points of the correlation function are measured by the correlator. Accordingly, only the weakly decaying tail of the second exponential is effective in the first few points of the measured corrleation function and is too small to contribute appreciably to the first cumulant. One also has to keep in mind that the influence of only a few dust particles will cause a decrease of the first cumulant, so that the observed decrease of D_{app} may also have its origin in this effect.

Conclusions

As shown in Table I the ρ values for polystyrene in toluene were found to be molecular weight independent but approximately 11% lower than predicted from the blob theory for polymers in a good solvent.[27] Deviations of the same height and in the same direction have been observed earlier with PMMA in acetone.[7] We can now be sure that these deviations are not caused by systematic errors.

We also tried to determine the coefficient C in eq 2. It has been shown[28] that this parameter depends on the experimental time scale. Accordingly, the reduced first cumulant has to be measured at different sampling times and extrapolated to zero time. We here attempted to do this for the F288 sample, and the result is shown in Figure 7. The zero time value of C is found to be about 0.2, although the experimental error is considerable at the two smallest sampling times, which are far away from the optimal sampling time suggested by Jakeman et al.[10] If we take into account the reported polydispersity, we predict from theory[2] that $C = 0.181$, which is within the experimental error of the observed value. The influence of excluded volume on the magnitude of C is not known, but first calculations with low excluded volumes (perturbation theory) show no noticeable effect.[29]

In summary, we can state that simultaneous static and dynamic light scattering can be carried out with high accuracy. This high accuracy may be surprising at first sight, since the conditions for optimization of both techniques are mutually exclusive (small scattering volume for QLS but large for ILS). Actually, our results demonstrate the poor construction of conventional light scattering instruments. In fact, for instance, the instrument designed by Fujita et al.[30] yields static light scattering results of a much higher accuracy than can ever be obtained with our photon correlation spectrometer. Nevertheless, the advantage of simultaneous static and dynamic light scattering is obvious.

Acknowledgment. We are grateful to Professor B. Chu, University of New York at Stony Brook, who kindly scrutinized our old commercial spectrometer in 1977, thus initiating the present reconstruction of the apparatus. A valuable suggestion by a referee to apply the Mie scattering theory to our ILS data is kindly acknowledged. We are indebted to Mr. W. H. Peters, ALV-Laser Vertriebsgesellschaft m.b.H., Langen, for helpful discussions. For the accurate manufacture of the various mechanical parts we thank the workshop of our institute, especially Mr. B. Machutta. Fa. Volpi, Denzlingen, kindly provided us with two light conducting cables. Financial support of this work by the Deutsche Forschungsgemeinschaft is kindly appreciated.

Appendix

The normalized correlation function of a polydisperse spherical rigid system is given by[22]

$$g_1(t) = \sum_k B_k \exp(-q_k^2 D_k t) / \sum_k B_k \qquad \text{(A1)}$$

where $B_k = m_k M_k P_k(q)$, m_k is the mass fraction of the kth component, and M_k is the molecular weight of the kth component. For the special case of back-scattering occurring for a monodisperse system, we deal with two exponentials with the following conditions: $m_1 = m_2$, $M_1 = M_2$, $D_1 = D_2$, $P_1(q) = P(q)$, $P_2(q) = P(q^*)$, $q_1 = q$, and $q_2 = q^*$. Thus, having taken care of the lower intensity of the reflected beam, one obtains

$$g_1(t) = P_g^{-1}[P(q) \exp(-q^2 D t) + P(q^*)(I_r/I_p) \exp(-(q^{*2}/q^2) D t)] \qquad \text{(A2)}$$

where I_r/I_p is the ratio of the reflected to the primary light intensity and $P_g = P(q) + P(q^*)$. According to the definition of the first cumulant

$$\Gamma = -\lim_{t \to 0} \mathrm{d}(\ln [g_1(t)])/\mathrm{d}t \qquad \text{(A3)}$$

we arrive after some manipulations at the final result.

$$\Gamma/(q^2 D) = D_{app}/D = P_g^{-1}[P(q) + P(q^*)(I_r/I_p)(q^{*2}/q^2)] \qquad \text{(A4)}$$

References and Notes

(1) See, for example: (a) Chu, B. "Laser Light Scattering"; Wiley: New York, 1974. (b) Cummins, H. Z.; Pike, E. R. "Photon Correlation and Light Beating Spectroscopy"; Plenum Press: New York, 1974. (c) Cummins, H. Z.; Pike, E. R. "Photon Correlation Spectroscopy and Velocimetry"; Plenum Press: New York, 1977. (d) Degiorgio, N.; Cati, M.; Giglio, M. "Light Scattering in Liquids and Macromolecular Solutions"; Plenum Press: New York, 1980.
(2) Burchard, W.; Schmidt, M.; Stockmayer, W. H. *Macromolecules* **1980**, *13*, 1265.
(3) Yamakawa, H. "Modern Theory of Polymer Solutions"; Harper and Row: New York, 1971.
(4) Pyun, C. W.; Fixman, M. *J. Chem. Phys.* **1966**, *44*, 2107.
(5) Imai, S. J. *J. Chem. Phys.* **1969**, *50*, 2116.
(6) Yamakawa, H. *J. Chem. Phys.* **1962**, *36*, 2995.
(7) ter Meer, H.-U.; Burchard, W.; Wunderlich, W. *Colloid Polym. Sci.* **1980**, *258*, 675.
(8) Schmidt, M.; Burchard, W. *Macromolecules* **1981**, *14*, 210.
(9) Schmidt, M. Ph.D. Thesis, 1980, Freiburg.
(10) Jakeman, E. In "Photon Correlation and Light Beating Spectroscopy"; Cummins, H. Z., Pike, E. R., Eds.; Plenum Press: New York, 1974.

(11) Bantle, S. Ph.D. Thesis, 1982, Freiburg.
(12) Thurn, A. Diploma Thesis, 1982, Freiburg.
(13) ter Meer, H.-U.; Burchard, W., unpublished.
(14) Schmidt, M.; Burchard, W.; Ford, N. C. *Macromolecules* **1978**, *11*, 452.
(15) Supplied by: W. H. Peters, ALV-Laser Vertriebsgesellschaft m.b.H., Langen.
(16) Huber, K. Diploma Thesis, 1982, Freiburg.
(17) Dandliker, W. B.; Kraut, J. *J. Chem. Phys.* **1953**, *78*, 2380.
(18) Pike, E. R.; Pomeroy, W. R. M.; Vaughan, J. M. *J. Chem. Phys.* **1975**, *62*, 3188.
(19) Mächtle, W.; Fischer, W. *Angew. Makromol. Chem.* **1969**, *7*, 149.
(20) Berry, G. C. *J. Chem. Phys.* **1966**, *44*, 4550.
(21) Raczek, J.; Meyerhoff, G. *Macromolecules* **1980**, *13*, 657.
(22) Berne, B.; Pecora, R. "Dynamic Light Scattering"; Wiley: New York, 1976.
(23) Rayleigh, Lord *Proc. R. Soc. London, Ser. A* **1911**, *84*, 26.
(24) Gans, R. *Ann. Phys. (Leipzig)* **1925**, *76*, 29.
(25) Pangonis, W. J.; Heller, W. "Angular Scattering Functions for Spherical Particles"; Wayne State University Press: Detroit, 1960.
(26) Lüddecke, E., personal communication at the "Workshop on Photon Correlation Spectroscopy and Quasi-elastic Light Scattering Studies", Dreieich-Sprendlingen, 1981.
(27) Benmouna, M.; Akcasu, A. Z. *Macromolecules* **1978**, *11*, 1187.
(28) Schmidt, M.; Stockmayer, W. H. *Macromolecules*, submitted.
(29) Tanaka, G.; Stockmayer, W. H. *Macromolecules*, submitted.
(30) Einaga, Y.; Mitani, T.; Hashimoto, J.; Fujita, A. *Polym. J.* **1979**, *11*, 565.

Short-Time Behavior of the Dynamic Structure Factor for Flexible-Chain Molecules

Manfred Schmidt,† W. H. Stockmayer,* and Marc L. Mansfield‡

Department of Chemistry, Dartmouth College, Hanover, New Hampshire 03755.
Received August 17, 1982

ABSTRACT: The short-time behavior of the dynamic structure factor $S(q,t)$ for flexible Gaussian chains is discussed with the familiar Zimm model. Although the drift from initial to steady-state translational diffusion coefficient may not be observable, the angle-dependent term proportional to the fourth power of the scattering vector decays at a rate that may influence the evaluation of the first cumulant from photon correlation measurements.

In recent years, much valuable information on the dynamical behavior of dissolved flexible macromolecules has been obtained from measurements of quasi-elastic light scattering.[1,2] Attention has often been concentrated on the first cumulant Γ (initial time derivative) of the dynamic structure factor $S(q,t)$, both because it appears to be readily obtainable from experiment and because it can theoretically be expressed in terms of equilibrium averages over the macromolecular conformations. The latter circumstance was recognized by Akcasu and Gurol (hereafter AG)[3] and has been extensively utilized in the theoretical study of different molecular models.[3-11] The theoretical expression is sufficiently tractable so that premature averaging of the hydrodynamic interactions among the various parts of the dissolved macromolecule can often be avoided.

A possible difficulty in the evaluation of the true first cumulant from experiment is that the structure factor at short times contains contributions from all the chain coordinates, including some that decay very rapidly. Thus, because the time resolution of any photon-correlation apparatus is limited, there is a danger that the apparent first cumulant found experimentally will differ from the true initial value. In the limiting case of rigid molecules, most of the internal molecular modes become infinitely fast, and the problem just described becomes acute.[12]

At low scattering angles the first cumulant can be written as

$$\Gamma = q^2D[1 + Cq^2\langle S^2\rangle + ...] \qquad (1)$$

where D is the translational diffusion coefficient, $\langle S^2\rangle$ is the mean square radius of gyration, and the magnitude of the scattering vector is $q = (4\pi/\lambda)\sin(\theta/2)$. For polydisperse samples, both D and $\langle S^2\rangle$ are z-average values. The dimensionless coefficient C depends on chain structure (e.g., presence of branches[10] or rings[11]), on polydispersity,[10] and on chain stiffness,[13] but it is only slightly affected by excluded volume.[14] Perhaps more interestingly, its theoretical value depends[3,9] on whether the intrachain hydrodynamic interactions, as expressed in the customary Oseen–Kirkwood–Riseman formulation,[15,16] have been preaveraged or allowed their full range of fluctuating values. For the latter reason alone, a careful evaluation and full understanding of C is worth pursuing, and this pursuit is the principal goal of the present work.

Translational Diffusion

Because of coupling between translational and internal motions, the aforementioned short-time problem is already seen in the limiting low-angle term q^2D. The initial value necessarily corresponds to an unbiased equilibrium distribution of chain conformations and orientations (and to a corresponding theoretical equation for D originally derived by Kirkwood[17]), but eventually a steady-state value of D is reached in which the differing translational resistances of the various conformations are weighted accordingly.[18-20] For flexible chains the effect is most easily seen for the Zimm model,[21] where the hydrodynamic interactions are preaveraged and an analytical solution is possible. In this case the dynamic structure factor at low scattering vectors[22,23] can be expressed in the form

$$\ln[S(q,t)/S(q,0)] = -q^2tD(t) + \mathcal{O}(q^4) \qquad (2)$$

with

$$[D(t) - D(\infty)]/D(\infty) = \sum_{k=1} J_k^2\nu_k f(u_k)/J_0^2\nu_0 \qquad (3)$$

where $D(\infty)$ is the final steady-state diffusion coefficient, the ν_k are the eigenvalues of Zimm's hydrodynamic **N** matrix, and

† Present address: Institut für Makromolekulare Chemie, Universität Freiburg, D-7800 Freiburg, West Germany.
‡ Present address: Department of Chemistry, Colorado State University, Fort Collins, CO 80523.

0024-9297/82/2215-1609$01.25/0